Thermal Hydraulic Modeling of a Dry Cask and Microchannel

Spent Fuel and Waste Disposition

SUMMARY

Researchers at Pacific Northwest National Laboratory have completed an initial stage of work toward the development of a multiscale modeling capability with the Generation of Thermal Hydraulic Information in Containment (GOTHIC^{TM})[1] code to perform simulations for thermal hydraulic conditions within a spent nuclear fuel dry cask and postulated stress corrosion cracks. Model development and simulations performed in the initial stage demonstrate GOTHIC thermal hydraulic simulations of both microchannel particle flows and conditions within a modern dry cask storage system, based on NAC International (2015) Modular, Advanced Generation, Nuclear All-purpose STORage (MAGNASTOR), compare closely with known solutions.

Aerosol transport and deposition within a microchannel were simulated with pressure differentials as high as 700 kPa, which represent the expected range of dry cask operating pressures. Pressure-dependent flow through a microchannel was predicted to within 5 percent of that measured, up to a pressure differential of ~500 kPa, after which the error increased to 17 percent. GOTHIC was found to underpredict the deposition rate and the deposition rate was adjusted by 195 percent to 310 percent to match experimental measurements conducted by Sandia National Laboratories. The adjustments are admittedly large; however, this is attributable to the use of a water drop aerosol model to model a dry cerium-oxide aerosol. GOTHIC features a dry aerosol model; however, the code version used for this work (8.2) is affected by a known limitation and therefore could not be used.

GOTHIC was also used to simulate the heat removal performance and conditions within a modern dry cask storage system. The decay heat from each spent fuel bundle was simulated and transferred by conduction and convection out to the environment. Comparison of peak clad temperatures from the hot fuel bundle show excellent agreement with the independent results from STAR-CCM+ (CFD) and COBRA-SFS (finite volume) simulations.

The latest release of GOTHIC (Version 8.3) fixes the limitation affecting the dry aerosol model. This was confirmed by correspondence with the developers of GOTHIC. Despite adjustments to the deposition rate to match measurements, the general capability of GOTHIC and fundamental equations of the aerosol model warrant further evaluation with the latest release (Version 8.3).

The GOTHIC thermal hydraulic simulation framework shows promise of being able to model the complex environment of a dry cask storage system with aerosol flow and deposition within a microchannel volume having dimensions similar to a stress corrosion crack. Future research will refine both the aerosol and dry cask models to allow more accurate investigation and representation of the key experimental physics.

---

[1] GOTHIC^{TM} incorporates technology developed for the electric power industry under the sponsorship of the Electric Power Research Institute (EPRI).

This page is intentionally left blank.

ACKNOWLEDGEMENTS

This page is intentionally left blank.

CONTENTS

LIST OF FIGURES

LIST OF TABLES

ACRONYMS

BC	boundary conditions
CC	concrete cask
CFD	computational fluid dynamics
DCSS	dry cask storage system
GOTHIC	Generation of Thermal Hydraulic Information in Containments
MAGNASTOR	Modular Advanced Generation, Nuclear, All-purpose STORage
MFR	mass flow rate
ORNL	Oak Ridge National Laboratory
PCT	peak clad temperature
PNNL	Pacific Northwest National Laboratory
PWR	pressurized water reactor
Re	Reynolds number
SCC	stress corrosion crack
SNF	spent nuclear fuel
SNL	Sandia National Laboratories
DSC	dry storage canister

This page is intentionally left blank.

THERMAL HYDRAULIC MODELING OF A DRY CASK AND MICROCHANNEL

1.   INTRODUCTION

The potential consequences of the release of the contents of pressurized spent nuclear fuel (SNF) dry storage containers after the formation of through-wall breaches are of current concern as timelines for extended dry storage expand in the absence of a licensed geological repository. To address this concern experimental and modeling efforts have been focused on characterizing the transport of gases and suspended particulates through such breaches. Current studies are focused on the transport of aerosols through pinhole-size breaches with diameter, or width, less than 100 μm, which can develop in the primary containment boundary of SNF casks. Determination of the potential release via transport of aerosol and particulate matter through pinhole breaches relies on knowledge of the breach characteristics and the upstream conditions within a SNF cask.

This report presents and discusses the initial stage of work completed to develop a pinhole breach model and a separate SNF dry cask model. A pin-hole breach model is developed with the parameters of a microchannel experiment reported by Durbin et al. (2018). The modeling error is assessed by comparison of model predictions with experiment measurements for gas and aerosol flow and aerosol deposition in the microchannel.

A thermal-hydraulic model of a spent fuel cask is being developed to enable calculations for the distribution and state of aerosols within the cask environment, which eventually can be used to generate realistic conditions upstream to a pinhole breach. At this time, the model has been developed adequately to predict the hot bundle fuel peak clad temperatures (PCTs), cask internal gas temperature, and the radial distribution of natural convection velocities—predictions that are validated by comparison to calculations from independent analytical models developed by Fort et al. (2016).

This page is intentionally left blank.

2.   BACKGROUND

Dry cask storage systems for SNF are designed to encapsulate the SNF, prevent the release of radioactive material, and provide long-term removal of the SNF decay heat. Decay heat is transferred to the environment by convective cooling of the canister by airflow between the canister and storage cask. Particulates present in the airflow source will deposit on the canister surface, presenting a potential for localized corrosion by the pitting mechanism. Corrosion of the canister along with potential stresses can lead to pitting evolution and, eventually, stress corrosion crack (SCC) formation.

Previous thermal modeling of a SNF dry cask storage system investigated PCTs for fuel assemblies and structure temperatures (Fort et al. 2016). Detailed assembly calculations were performed with the COBRA-SFS thermal-hydraulic software, Version 5.0 (Michener et al. 2019). The model used radial- and axial-dependent, best-estimate and design-basis decay heat loads. Radial- and axial-dependent PCTs were calculated and were found to depend strongly on the cask boundary conditions: the ambient temperature, and to a lesser extent, magnitude of solar insolation. Fort et al. (2016) reported 301 °C PCT in the center assembly for the initial storage configuration with a total decay heat loading of 26.4 kW, as well as calculations of assembly PCT at times ranging 10 to 300 years.

Fort et al. (2016) also developed a Star-CCM+ computational fluid dynamics (CFD) model to investigate detailed steady-state flow and temperature distributions for the same initial loading configuration. CFD calculation results were 307 °C PCT with He flow velocities of 0.7-1.0 m/s in the downcomer annulus. Calculations showed nearly uniform velocity through the inner channels with counter-current flow occurring along the boundary within periphery channels.

Content release through pinhole breaches in storage containers is a concern that has existed since the original efforts to license the Yucca Mountain Geological Repository. The concern remains even after the decision was made to focus on interim and extended dry storage. A method for characterizing such breach scenarios was presented by Casella et al (2014), which assumed fully developed laminar flow through right circular cylindrical breaches in which Brownian diffusion was the only mechanism of particulate deposition within the breach. This model was a base case in which fundamental descriptions of carrier gas flow and particle transport were found applicable. Plans to expand the model to account for different flow regimes and breach geometries were not pursued due to lack of funding and interest associated with programmatic changes. However, renewed concerns over particulate releases through pinhole breaches in dry storage containers have led to work that has advanced the applicability of this phenomenological approach (Chatzidakis 2018). Additionally, experimental capabilities have been established and initial results have been gathered for particulate transport through breaches with geometric characteristics relevant to this modeling approach (Durbin et al. 2018).

The work presented in this report is an attempt to supplement these experiments and phenomenological models with analysis from a qualified, multiphase thermal-hydraulic engineering software package. In particular, the use of the Generation of Thermal Hydraulic Information in Containments (GOTHIC) code provides a general framework that will allow the coupling of the thermal-hydraulic conditions within the cask to the flow through the breach. This will allow a time-dependent characterization of the aerosol source term and an aerosol flow deposition within the breach.

This page is intentionally left blank.

3.   OBJECTIVE

The objective of this work is the development and validation of separate thermal-hydraulic models for a SNF dry cask storage system and a microchannel breach.

The microchannel model was developed based on experiments performed by Sandia National Laboratories (SNL) researchers (Durbin et al. 2018). The microchannel experiment was designed to capture phenomena of aerosol flow and retention in SCC. Development and validation of a microchannel model will enable detailed calculations for flow of vapor and aerosols dependent on the upstream pressure and aerosol concentration. Pacific Northwest National Laboratory (PNNL) has chosen to develop a microchannel model using the finite volume software GOTHIC to complement the finite difference models being developed at Oak Ridge National Laboratory (ORNL) by Chatzidakis (2018).

Anticipating the need to generate realistic conditions upstream to SCC, such as pressure, aerosol concentration, and size distribution, a new SNF cask model was developed based on a commercial dry cask storage system (DCSS). In this initial stage of work, validation of the cask model was established by comparing predicted PCT and natural circulation flows with independent analytical models. Modeling of aerosols within the cask with further validation of the model is planned for the next stage of work.

This page is intentionally left blank.

4.   THERMAL HYDRAULIC CODE

GOTHIC is an integrated finite volume, general-purpose thermal-hydraulics software package for design, licensing, safety, and operating analysis of nuclear power plant containment, confinement buildings, and system components (GOTHIC, 2016). GOTHIC has a broad set of capabilities and is highly customizable through the use of internal control variables, coupling with external models, and dynamic library linking.

4.1   Code Capability

GOTHIC is a finite volume computer program that solves the conservation equations for mass, momentum, and energy for multicomponent, multiphase flow in complex geometries. The phase balance equations are coupled by mechanistic models for interface mass, energy, and momentum transfer that cover the entire flow regime from bubbly flow to film/drop flow, as well as single-phase flows. The phase interface models allow for the possibility of thermal nonequilibrium between phases and unequal phase velocities, including countercurrent flow. The GOTHIC solver (GOTHIC_S) includes full treatment of the momentum transport terms in multidimensional models, with optional models for turbulent shear and turbulent mass and energy diffusion. Conservation equations are solved for three primary fields:

- Steam/gas mixture
- Continuous liquid
- Liquid droplet fields.

4.2   Aerosol Modeling with GOTHIC

Aerosols are represented with drop fields in GOTHIC and any number of drop fields may be used to simulate drop behavior. Each drop field presents a lognormal size distribution, which is characterized by a median diameter and geometric standard deviation. Drop field source terms include drop creation (injection, jet and drop breakup, and creation from mist), agglomeration, deposition, entrainment, dripping, evaporation, and condensation.

The drop momentum equation includes drop drag, which influences the drop mobility relative to the vapor phase and other drops. The effective drag is calculated with correlations for viscous, solid sphere, and distorted drop regimes. The net result is that drops may have a different velocity than the surrounding vapor.

GOTHIC Version 8.3 provides the capability to simulate dry aerosol fields based on the drop field model, where the dry aerosols are carried as solid components suspended in the drop field. This capability is not available in Version 8.2, which was used in this work. Although the dry aerosol capability was not available, the drop field represents a wet aerosol with the capabilities described above, which may be used as a surrogate for dry aerosol, and the authors took this approach. A shortcoming of the approach to modeling a dry aerosol as the water drop field is phase change, particularly drop evaporation. GOTHIC is a multiphase, integrated code that tracks thermodynamic properties and solves the multiphase interface mass and energy transfers, which are essential to solving problems involving multiphase flows. The capability to shut off drop evaporation does not exist; however, the effect can be minimized by minor adjustments to the model conditions.

4.3   GOTHIC Deposition Model

GOTHIC 8.2 (GOTHIC 2016) droplet deposition based upon the droplet concentration gradient and a calculated deposition velocity

$$\gamma_d^{"} = k_d(c_d - c_w)$$

<div align="right">Eq. 1</div>

Where

$\gamma_d^{"}$ is deposition flux, $\left(\frac{\text{kg}}{m^2\text{-s}}\right)$

k_d is the deposition velocity $\left(\frac{m}{s}\right)$

c_d is the droplet bulk particle concentration $\left(\frac{\text{kg}}{m^3}\right)$

c_w is the wall particle concentration $\left(\frac{\text{kg}}{m^3}\right)$, this is assumed to be zero for the calculation of deposition velocity.

The droplet bulk particle concentration is defined as

$$c_d = \frac{\alpha_d v_d}{\alpha_d v_d + \alpha_v v_v}\rho_d$$

<div align="right">Eq. 2</div>

Where

α_d is volume fraction of droplets in the vapor phase[2]

v_d is the velocity of the droplets in the vapor phase $\left(\frac{m}{s}\right)$

α_v is volume fraction of vapor

v_v is the velocity of the vapor phase $\left(\frac{m}{s}\right)$

ρ_d is the density of the droplets $\left(\frac{\text{kg}}{m^3}\right)$.

The deposition velocity is a function that includes (GOTHIC 2016)

$$k_d = 0.0889 Sc^{-0.704}\sqrt{\frac{f}{2}}v_v$$

<div align="right">Eq. 3</div>

Where

Sc is Schmidt number, the ratio of viscous to mass diffusion

f is the Fanning friction factor.

The Schmidt number may be given by

---

[2] When referring to droplets in the vapor phase, the authors mean a mixture of drops, steam, and non-condensable gases.

$$Sc = \frac{\mu_v}{\rho_v D_b} \qquad \text{Eq. 4}$$

Where

μ_v is the vapor dynamic viscosity (Pa-s)

ρ_v is the density of the vapor $\left(\frac{\text{kg}}{m^3}\right)$

D_b is the thermal diffusion coefficient $\left(\frac{m^2}{s}\right)$.

Thermal diffusion coefficient is based upon Brownian motion (Hinds 1982)

$$D_b = \frac{K_B T_v C_c}{3\pi \mu_v d_p} \qquad \text{Eq. 5}$$

Where

K_B is the Boltzmann constant, $1.38065812 \times 10^{-23} \left(\frac{J}{K}\right)$

T_v is the vapor temperature (K)

d_p is the particle diameter (m)

C_c is the Cunningham correction factor.

The Cunningham correction factor is used to account for slip between gas and very small particles

$$C_c = 1 + \frac{\lambda}{d_p}\left(2.514 + 0.8e^{-0.55\frac{d_p}{\lambda}}\right) \qquad \text{Eq. 6}$$

Where

λ is mean free path of the gas (m).

The gas mean free path is a function of molecular concentration and collision diameter

$$\lambda = \frac{1}{\sqrt{2}n\pi d_m{}^2} \qquad \text{Eq. 7}$$

Where

n is the molecular concentration $\left(\frac{\text{atoms}}{m^3}\right)$

d_m is the molecular collision diameter (m).

For an ideal gas the molecular concentration is

$$n = \frac{N_A P}{R T_v} \qquad \text{Eq. 8}$$

Where

N_A is Avogadro's number, $6.602136736 \times 10^{23} \left(\frac{\text{molecules}}{mol}\right)$

R is the gas constant, $8.31451070 \left(\frac{J}{\text{mol-K}} \right)$

P is the gas pressure (Pa).

The collision diameter for nonattracting molecules is (Hirschfelder et al. 1954)

$$d_m^2 = \frac{5 \sqrt{\frac{MW_v R T_v}{\pi}}}{16 N_A \mu_v}$$

Eq. 9

Where,

MW_v is the vapor molecular weight $\left(\frac{kg}{\text{mol}} \right)$.

4.4 Applicability of GOTHIC Deposition Model

Casella (2014) presents a model of deposition of particulate flow through cracks. This model will be briefly compared to the GOTHIC formulation to verify applicability.

For a one-dimensional flow in a straight tube with radial coordinates reference, Casella presents a simplified continuity equation with only convective and diffusive terms

$$(1 - \hat{r}^2) \underbrace{\frac{\partial \hat{n}}{\partial \hat{x}}}_{\text{Axial Gradient}} = \underbrace{\frac{1}{Pe}}_{\text{Brownian Diffusion}} \underbrace{\frac{1}{\hat{r}} \frac{\partial}{\partial \hat{r}} \left(\hat{r} \frac{\partial \hat{n}}{\partial \hat{r}} \right)}_{\text{Radial Gradient}}$$

Eq. 10

Where

$\hat{r} = \frac{r'}{r}$ is relative radial position

r' is radial position (m)

r is crack radius (m)

$\hat{x} = \frac{x}{L}$ is relative axial position

x is axial position within the crack (m)

L is the crack length (m)

$\hat{n} = \frac{n}{n_0}$ is relative particle concentration

n is particle concentration $\left(\frac{\text{atoms}}{m^3} \right)$

n_0 is the particle concentration in the cask $\left(\frac{\text{atoms}}{m^3} \right)$

Pe is the Péclet number comparing convection to conduction.

For Eq. 10, the first boundary condition sets the normalized inlet concentration to unity

$$\hat{n}(\hat{r}, 0) = 1$$

Eq. 11

For Eq. 10, the second boundary condition sets the particle concentration at the wall boundary to zero

$$\hat{n}(1, \hat{x}) = 0$$

Eq. 12

The Péclet number for this scenario may be simplified to

$$Pe = \frac{rU}{D_b}$$

<div align="right">Eq. 13</div>

Where

U is maximum velocity for fully developed laminar flow $\left(\frac{m}{s}\right)$

Casella (2014) concludes that if the flow is laminar and fully developed, "that the particles being carried through the breach are small enough that their motion is influenced only by the convective motion of the carrier gas and Brownian diffusion."

Therefore, one may conclude that GOTHIC and Casella use similar diffusive mechanisms. The similarities between the approaches are:

- Assumed complete particle capture at wall surfaces (zero concentration of particles in the vapor phase at the wall).

- Particle motion is described by carrier gas convection and Brownian diffusion (with Cunningham slip) and deposition is governed by particle diffusion to the pathway wall.

A few differences between the approaches are:

- GOTHIC calculates the velocity in each solution node allowing for turbulent or laminar flow instead of using the Poiseuille equation. In practice, GOTHIC calculates laminar flow at the conditions of interest.

- GOTHIC allows the droplets and vapor to have different velocities. In practice, these velocities are likely to be nearly identical at the small particle sizes of interest.

- GOTHIC calculates additional deposition mechanisms not mentioned here (e.g., turbulent diffusion, thermophoresis, and diffusiophoresis). In practice, thermal diffusion due to Brownian motion will dominate in the conditions of interest and to some degree these other mechanisms can be disabled through user input options.

- GOTHIC Version 8.2 effectively only supports liquid water droplets instead of the desired solid cerium oxide particles used in the validation basis of this work (Section 5.2). This is due to a known limitation in Version 8.2 coding that has been rectified in Version 8.3.

This page is intentionally left blank.

5. MICROCHANNEL MODEL

5.1 Microchannel Experiment

A thermal hydraulic model of a microchannel was developed based on the microchannel experiment conducted by Durbin et al. (2018) to measure aerosol transport and retention in a microchannel. A microchannel test section was constructed using gauge blocks engineered with characteristic dimensions similar to those of a SCC. Microchannel geometry is summarized in Table 5-1.

Table 5-1 Microchannel Volume Parameters

Microchannel volume	3.15 E-9 m^3
Width	12.7 mm
Length	8.86 mm
Height	28.9 um
Hydraulic diameter	57.7 um

The depressurization of a SNF cask with flow through a microchannel was represented by a 0.908-m^3 pressurized tank loaded with an aerosol of surrogate material and an instrumented test section. The test apparatus is shown in Figure 5.1. Cerium oxide (CeO$_2$) was chosen as the surrogate material for oxide SNF due to a relatively high density (ρ_{CeO2} = 7.22 g/cm^3) and its commercial availability.

Flow from the tank into the test section was measured with a mass flow meter. Aerosol size and distribution were measured upstream and downstream to the microchannel with aerodynamic particle sizer (APS) spectrometers. Aerosol retention in the microchannel was determined by comparing the upstream and downstream aerosol concentrations.
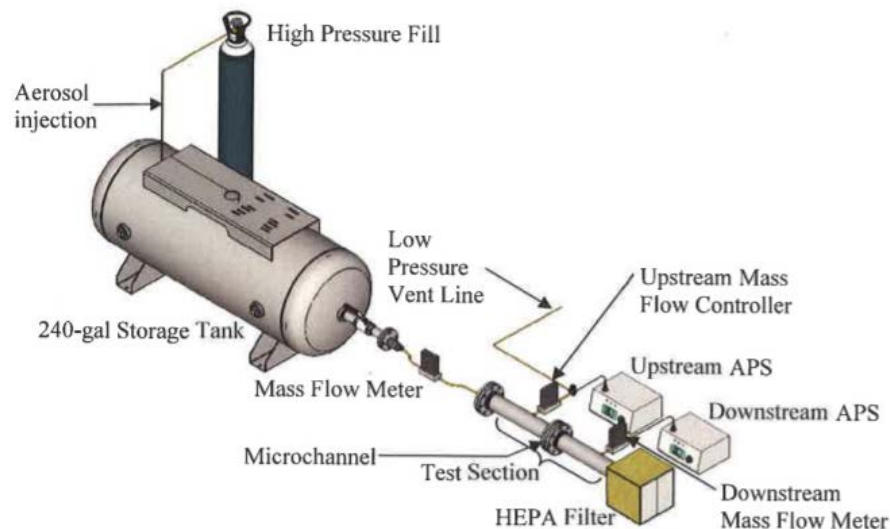
Figure 5.1 Experiment Apparatus from Durbin et al. (2018)

Figure 5.2 shows the particle size distribution of the surrogate aerosol used in the SNL tests. Here, the distribution is plotted as a function of aerodynamic equivalent diameter (AED).
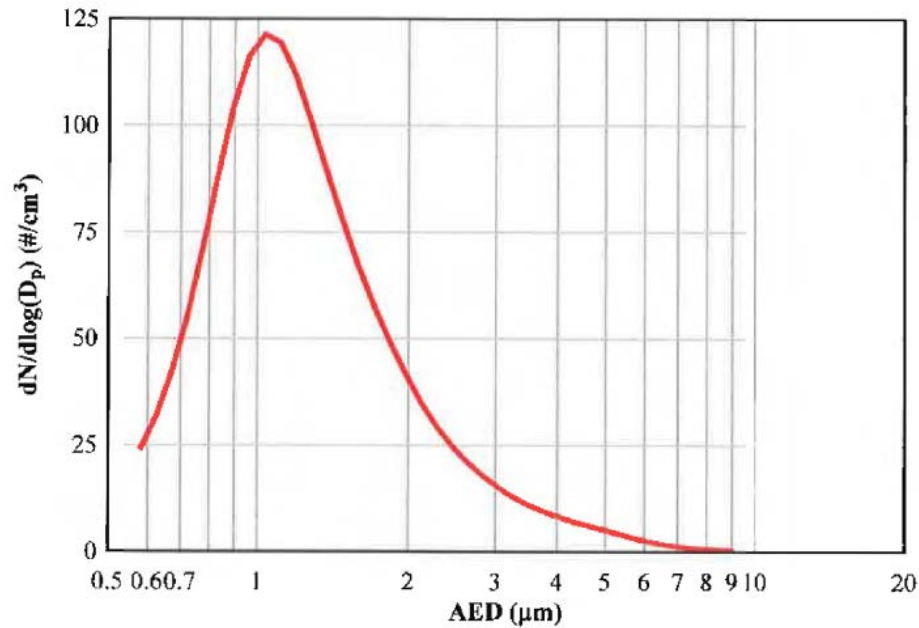
Figure 5.2 Particle-size Distribution of the Cerium Oxide Surrogate

5.2   Microchannel Model

A high-level schematic of the GOTHIC model is shown in Figure 5.3. The model consists of a 1d finite volume for the microchannel (shown as 1s), upstream boundary condition (BC, shown as 1P) representing the upstream pressure and flow conditions, a downstream pressure BC (2P) representing the ambient pressure condition, and hydraulic junctions (1 and 2), which connect the BC to the microchannel volume.

Figure 5.3 Microchannel Model Schematic

The microchannel volume was modeled as a 1d finite-volume, discretized along the length into five equal 1.772-mm cells, as shown in Figure 5.4 (not to scale). The inlet and exit junction connections are shown as 1a and 2a in the first and last nodes, respectively. The rectangle labeled 1s represents the location of a thermal structure, which is spanned evenly across the volume, representing the fluid to gauge block interface. Heat transfer from the fluid to the microchannel gauge blocks is expected to be minimal because the gauge block outer and inner surfaces are in contact with the fluid, however sensitivities are investigated.

Figure 5.4 Microchannel Discretization

5.2.1   Boundary Conditions

Several versions of the microchannel model were constructed to investigate microchannel flow dependence on differential pressure, minor pressure drop losses associated with non-uniformities in the flow channel, and laminar friction, as well as drop deposition and evaporation rates. Separate models were developed with pressure and flow BC upstream to the microchannel, however the same pressure BC (101 kPa) was used to represen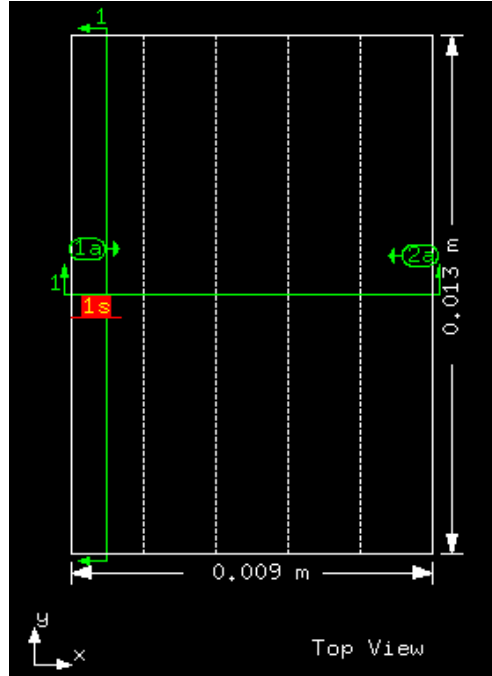t the downstream ambient conditions in each model. An assumed temperature of 25 °C was used for all BC (and initial conditions).

A pressure-pressure BC model allowed fast calculations for the steady state flow solution including the fluid velocity and property distribution along the microchannel length. Calculations were performed for upstream pressures ranging up to 801 kPa (maximum pressure differential of 700 kPa).

A flow-pressure BC model was convenient for estimating the deposition rate fraction from pseudo-steady state solutions (constant flow area and no deposition history). The air mass flow rate and microchannel inlet aerosol concentration were supplied by the measured data, shown in Figure 5.5.

Aerosol concentration, shown in Figure 5.5, represents the mass of aerosol occupying the gas volume. The aerosol concentration is represented as a liquid drop field in this model, supplied as the input of time dependent volume fraction of aerosol in the upstream mixture of air and aerosol. The liquid volume fraction is assumed to be 100 percent drops, characterized by the aerosol size distribution shown in Figure 5.2. The volume fraction of drops in the inlet air flow was calculated as the ratio of aerosol concentration to the material density of cerium oxide (7.22 g/cm^3) in Eq. 14

$$\alpha_l = \frac{\dfrac{C_{CeO2}(t)V_T}{\rho_{CeO2}}}{V_T} = \frac{C_{CeO2}(t)}{\rho_{CeO2}} \qquad\qquad \text{Eq. 14}$$

Where
$\quad\alpha_l$ = liquid volume fraction

$C_{CeO2}(t)$ = time-dependent cerium oxide aerosol concentration (kg/m³)
ρ_{CeO2}= cerium oxide density (kg/m³)
$C_{CeO2}V_T$ = upstream volume

The drop fraction α_d is equal to 1 (i.e., the liquid is 100 percent drops).
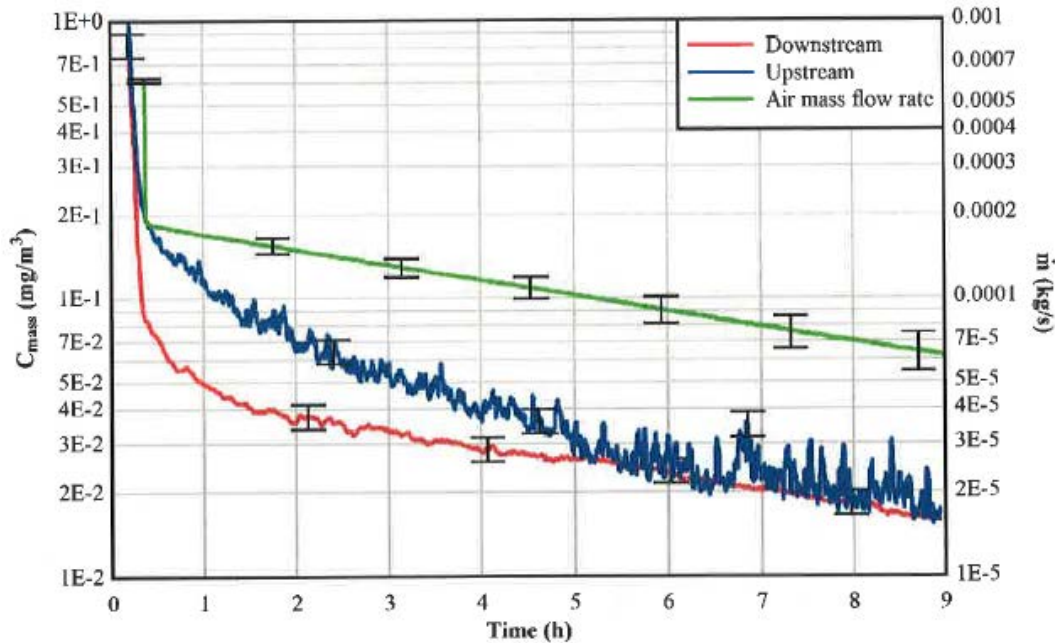
Figure 5.5 Measured Flow Rate in Microchannel and the Upstream and Downstream Aerosol Concentration (Durbin et al. 2018). Error bars indicate the measurement margin of error.

Upstream BC inputs are summarized in Table 5-2. The initial upstream concentration and flow at time t = 0 hour is not clear from Figure 5.5, therefore no attempt was made to compare model predicted values at time = 0 hour in the present work. Steady state calculations were performed for the set of BC parameters at each time period (i.e., 1 through 9 hours). The downstream BC input was 101.3 kPa pressure in all cases and the temperature was inconsequential since this BC was merely a sink.

Table 5-2 Model Upstream BC Inputs

Time (h)	Air MFR (kg/s)	Pressure (kPa)	Upstream aerosol concentration (kg/m³)	Downstream aerosol concentration (kg/m³)[a]	Drop volume fraction (Eq. 11)
1	1.71E-04	665.5	1.22E-07	5.45E-08	1.69E-11
2	1.52E-04	612.8	7.82E-08	3.93E-08	1.08E-11
3	1.34E-04	560.1	5.06E-08	3.05E-08	7.01E-12
4	1.17E-04	524.1	3.55E-08	2.61E-08	4.91E-12
5	1.03E-04	489.0	2.90E-08	2.46E-08	4.01E-12
6	9.04E-05	453.9	2.72E-08	2.41E-08	3.77E-12
7	7.95E-05	435.4	2.63E-08	2.29E-08	3.64E-12
8	7.03E-05	392.9	2.23E-08	1.92E-08	3.09E-12
9	6.30E-05	373.5	1.14E-08	1.13E-08	1.58E-12

[a]Downstream aerosol concentration is not a calculation input but provided here for comparison.

MFR = mass flow rate

5.2.2   Hydraulic Parameters

Hydraulic connections (referred to as flow paths in GOTHIC) connect the microchannel volume with the upstream and downstream BCs. These hydraulic parameters typically represent physical components, based on available dimensions such as pipe inner diameter, length, etc.; however, such detailed information from the experiment was not available. For this initial simple model, the microchannel dimensions for width, area, and hydraulic diameter were used as junction parameters. Reasonable pressure drop form loss coefficients ($0<K_L<3$) were found to provide good results. Form loss coefficients are correlated with flow area and direction changes that cause unrecoverable pressure losses.

5.2.3   Compressible Flow Dynamics

An important feature of the SNL experiment is the high-pressure differentials imposed on the microchannel. Adiabatic isentropic flow of an ideal gas in a convergent nozzle is given by (Chapman and Walker 1971) Eq. 15, where k =1.4 for air. The choking plane location within the microchannel can be estimated from Eq. 15 when P* is compared with the pressure drop solution through the channel. Assuming air as an ideal gas, the pressure ratio (P^*/P_0) equals 0.528. For a maximum downstream pressure of 101.325 kPa, the minimum upstream pressure necessary for choked flow without considering losses from friction or drag is 191.8 kPa, representing a pressure drop of 90.5 kPa.

$$\frac{P^*}{P_0} = \left(\frac{2}{k+1}\right)^{k/(k-1)}$$

Eq. 15

Note that Eq. 15 and Eq. 16 are applied on a per-node basis by the GOTHIC simulation code. By having multiple axial nodes, each node will have different fluid conditions as upstream nodes experience friction and potentially choking. As the pressure drops along the length of microchannel (parallel to flow direction), the downstream nodes will decrease in vapor density and there will be increased fluid velocity and frictional losses. The lengthwise distribution of friction losses will affect the choking location.

Pressure drop through the microchannel is dominated by friction, however the maximum achievable mass flow rate is limited by the sonic velocity in compressible air, assuming choking occurs. Assuming the flow of air is isentropic, the maximum mass flow rate of air in the microchannel is estimated closely by Eq. 16 (Chapman and Walker 1971). The actual flow may be further reduced by frictional losses.

$$\dot{m}_{max} = A\sqrt{\frac{k}{R}\left(\frac{2}{k+1}\right)^{(k+1)/(k-1)}}\frac{P_0}{\sqrt{T_0}}$$

Eq. 16

Where

R = gas constant for air 287.05 (J/kg K)

P_0 = upstream pressure ~801325 (Pa)

T_0 = stagnation temperature assumed 300 (K)

A = microchannel flow area 3.670e-7 (m²).

Eq. 16, plotted in Figure 5.6, shows that mass flow rate in the choked regime is proportional with the upstream pressure.
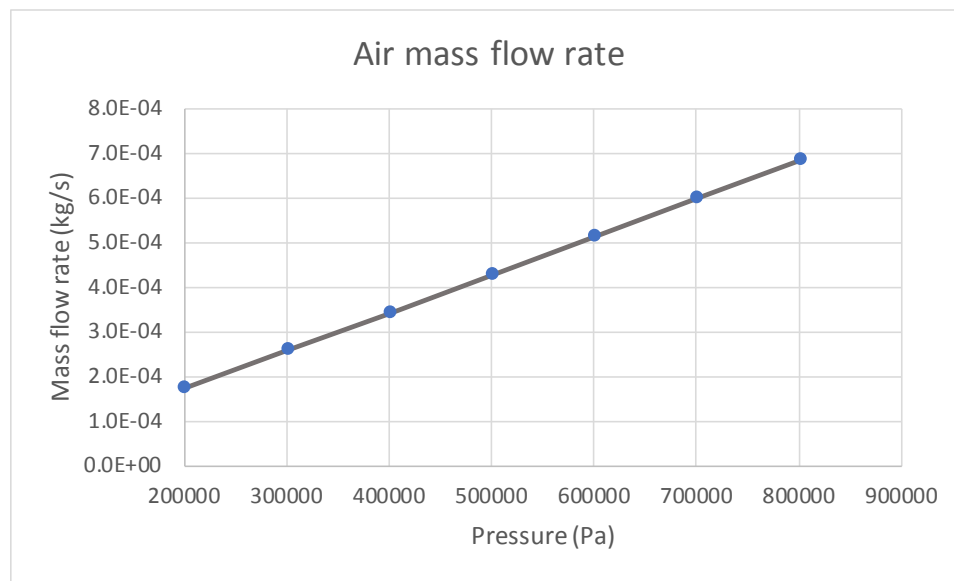
Figure 5.6 Isentropic Choked Mass Flow Rate of Air

5.2.4 Flow Conditions in Microchannel Flow

At very small values of the hydraulic diameter, the apparent behavior of gases departs from the continuum assumption. Typical analytic correlations for a continuum gas are not expected to be applicable when $D_h/\lambda_{mfp} \leq 10$ (Incropera et al. 2007). The mean free path (λ_{mfp}) for dry air at standard temperature and pressure (STP) is 65.4 nm (Jenkins 1988). In this work the typical analytic correlations for a continuum gas are assumed to be applicable as $D_h/\lambda_{mfp} > 100$, as shown here:

$$\frac{D_h}{\lambda_{mfp}} = \frac{5.58 \times 10^{-05}(m)}{65.4 \times 10^{-09}(m)} = 853$$

Laminar friction factors for circular and noncircular ducts are summarized in Table 5-3, where f is the Moody friction factor. The rectangular microchannel aspect ratio, defined as width/height, is 439.4. Comparing the microchannel aspect ratio with those correlated with laminar geometry factors in Table 5-3, the aspect ratio approaches the parallel plate condition of $f \cdot Re = 96$, where Re is the Reynolds number. Re is calculated for each cell in GOTHIC, followed by the calculation of f.

GOTHIC calculates the friction pressure drop with Eq. 17.

$$\Delta P = \frac{1}{2} \frac{f \Delta x}{D_h} \rho u_x{}^2 \qquad \qquad \text{Eq. 17}$$

Where

  f = Moody friction factor
  Δx = cell width
  u_x = velocity of fluid in x-direction.
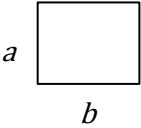
Table 5-3 Friction Factors for Fully Developed Laminar Flow (Incropera et al. 2007)

Cross Section	$\frac{b}{a}$	fRe_{D_h}
Circle	-	64
Square/rectangle	1.0	57
	1.43	59
	2.0	62
	3.0	69
	4.0	73
	8.0	82
	∞	96

5.2.5   Aerosol Modeling

For initial testing only the thermal diffusion mechanism of deposition is activated in calculations. Deposition from thermal diffusion is calculated as discussed in Section 4.3. The deposition rate can be adjusted by a scalar multiplier (applied to Eq. 1) to calibrate the rate if desired. The rate was adjusted to match the GOTHIC breakthrough fraction to the instantaneous breakthrough fraction from measurements. The breakthrough fraction is defined as the microchannel exit concentration of aerosol (or drops) divided by the inlet concentration

$$breakthrough\ fraction \equiv \frac{C_o}{C_i}$$

Steady state calculations were performed with the pressure and flow conditions in Table 5-2. These conditions were measured continuously during nine hours of tank blowdown and flow through the microchannel, including the aerosol concentration at upstream and downstream locations. In each calculation the deposition rate was adjusted to yield target breakthrough fractions, summarized in Table 5-4. Aerosol breakthrough fractions are derived from the aerosol performance data in Table 5-2.

Table 5-4 Breakthrough Fractions from Experiment

Time (h)	Aerosol breakthrough
1	44.6%
2	50.3%
3	60.2%
4	73.7%
5	84.9%
6	88.7%
7	87.2%
8	86.2%
9	99.0%

5.2.6   Results and Discussion

GOTHIC calculations of the microchannel mass flow rate are compared to the measured flow in Figure 5.7. The predicted mass flow rate is within 5 percent of that measured up to a pressure differential of ~500 kPa, after which the error increases to 17 percent (underpredicted) at the maximum differential (700 kPa).

Flow and pressure data from GOTHIC and measurement are plotted again in Figure 5.8, however in this plot the SNL data are split into two curves, fit by a linear curve above $\Delta P = 310$ kPa, and a quadratic curve below. The fits are very good, just as the quadratic fit over all the SNL data in Figure 5.7. This suggests that data are not sufficient to conclude what the true relationship is for mass flow rate above $\Delta P = 310$ kPa. The results are not inconsistent with the possible existence of choked flow in the appropriate pressure range, which would result in a linear relationship in the choked regime.

Choked flow is dependent on the upstream pressure, compressibility, geometry, and temperature. Thus, for constant area isentropic flow, the mass flow rate is dependent on the upstream pressure. Mass flow rate of air at less than sonic velocity depends on minor losses and friction forces that are proportional to the velocity squared. Therefore, based on first principles, one expects the transition from linear to nonlinear to occur at the minimum choking pressure.

Several sensitivity cases were carried out to reproduce the measured flow and pressure as shown in Figure 5.7. Some cases indicated that changes in the upstream temperature and the conditions in the aerosol sampling channels yielded results that appeared similar to Figure 5.7.

Relative to SNL experimental data, GOTHIC predicts the mass flow rate within 17 percent, although at lower pressure differentials, the error is less than 5 percent. GOTHIC appears to predict transitions in the flow regime not observed in experiments, but which have a physical basis, as discussed. Further work is needed to understand the experiment parameters and refine the model to better evaluate the model capability.
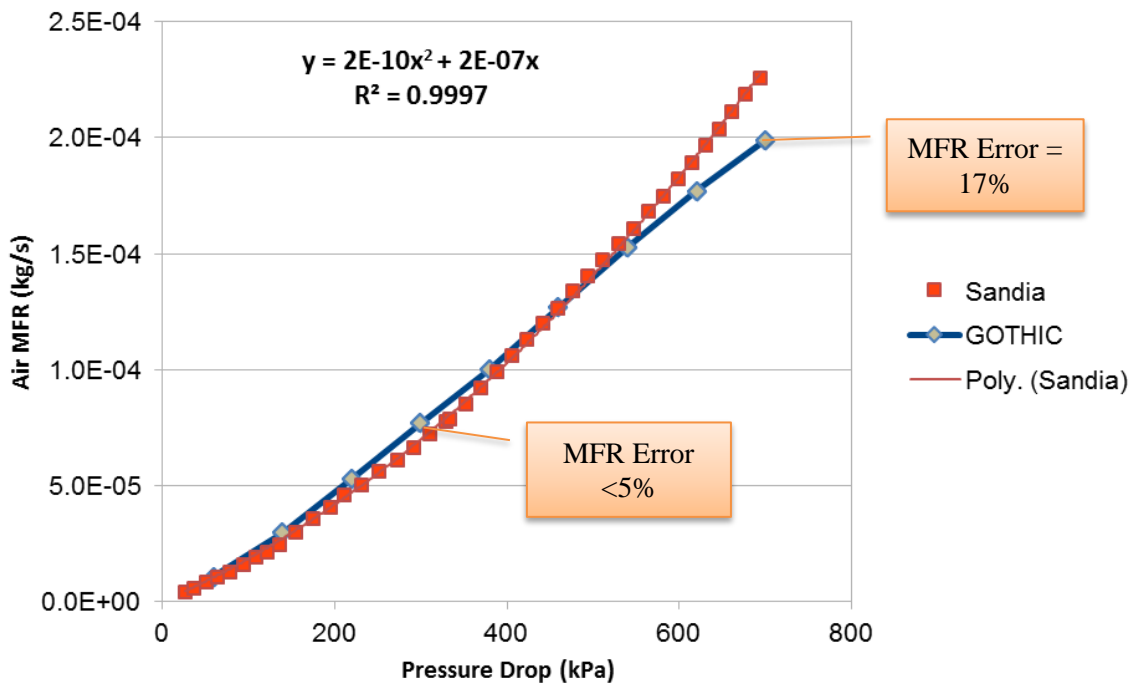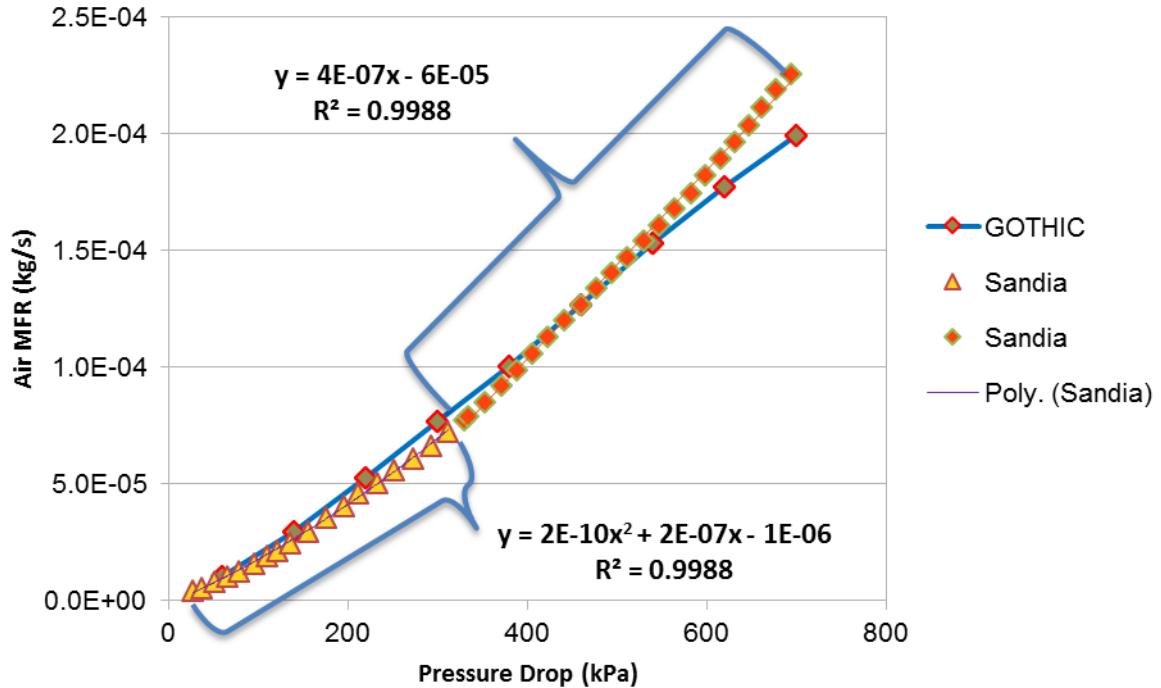
Figure 5.7 Microchannel Pressure Drop

Figure 5.8 Pressure and Flow Relationship

The deposition rate of aerosol in the microchannel was modeled with steady state calculations using pressure and flow conditions sampled at different times from the experimental blowdown of the tank. The pressure and flow conditions are shown in Table 5-5. In each case the upstream pressure, air mass flow rate, and aerosol concentration were provided as boundary conditions to the finite volume microchannel.

A controller was configured to adjust the deposition rate with a multiplier to tune the overall rate to match the breakthrough fraction, as discussed in Section 5.2.5. The following assumptions were made in this approach.

- The drop mass is based on the density of water, not cerium oxide. Cerium oxide is roughly seven times denser than water. This is a limitation of GOTHIC Version 8.2.

- The drop field undergoes phase change by vaporization. This was limited to the extent possible.

- Aerosol deposition is based on deposition to a "clean" microchannel (i.e., no dependence on deposition history such as buildup). No attempt was made to correlate deposition with buildup or a change in flow area.

- Deposition of aerosol occurs only on the microchannel surfaces. Deposition outside the microchannel is not accounted for. Deposition in the apparatus outside of the microchannel in some amount is expected, however the relative amount is unknown.

- Deposition transport occurs only by Brownian diffusion. Other deposition mechanism models including settling, thermophoresis, and diffusiophoresis were not activated.

- Drops do not reentrain after deposition and the effect of agglomeration is neglected. Both reentrainment and agglomeration are not expected to be the same for water and cerium oxide. Furthermore, the role of these mechanisms in the experiment is considered minimal.

Deposition rates at each pressure and flow condition are listed in Table 5-5. Note that deposition rate multipliers were adjusted to reach agreement with experiment breakthrough fraction. The maximum rate multiplier was 3.10 (i.e., GOTHIC underpredicts the deposition rate by a factor of 3.10 at most). The deposition rates provided in Table 5-5 are equal to the thermal diffusion deposition rate calculated by GOTHIC, multiplied by the deposition rate multiplier.

The experimental breakthrough fractions (see Table 5-4) were used as target values to determine the deposition rate factor resulting in calculation of the target breakthrough. The breakthrough convergence error is small (<1%) but non-zero, therefore the calculated breakthrough is not exactly the same as measurement derived values.

Aerosol deposition and breakthrough fractions are shown in Figure 5.9 with the mass flow rate of air. The deposition rate parameter was adjusted based on the corrected breakthrough flow, assuming the evaporated drops would have passed through the microchannel. The necessary deposition adjustment was found to increase with the air mass flow rate, appearing to asymptotically approach a value slightly more than 3.0. Deposition appears to decrease as the mass flow rate decreases with time.

Table 5-5 Flow Conditions and GOTHIC Deposition Rate Parameters

| Transient Time (h)	Air MFR (kg/s)	Pressure (kPa)	Upstream aerosol concentration (kg/m3)	Breakthrough fraction adjusted for evaporation	Deposition Rate (kg/s)	GOTHIC dep. rate multiplier
1	1.714E-04	665.469	1.22E-07	42.23%	2.04E-13	3.10
2	1.517E-04	612.805	7.82E-08	48.83%	1.12E-13	3.05
3	1.337E-04	560.139	5.06E-08	59.84%	5.45E-14	2.94
4	1.175E-04	524.104	3.55E-08	72.98%	2.45E-14	2.75
5	1.031E-04	488.994	2.90E-08	83.78%	1.13E-14	2.54
6	9.039E-05	453.884	2.72E-08	88.29%	7.21E-15	2.40
7	7.949E-05	435.402	2.63E-08	86.91%	7.27E-15	2.44
8	7.035E-05	392.887	2.23E-08	85.94%	6.23E-15	2.47
9	6.297E-05	373.477	1.14E-08	97.54%	5.23E-16	1.95

MFR = mass flow rate
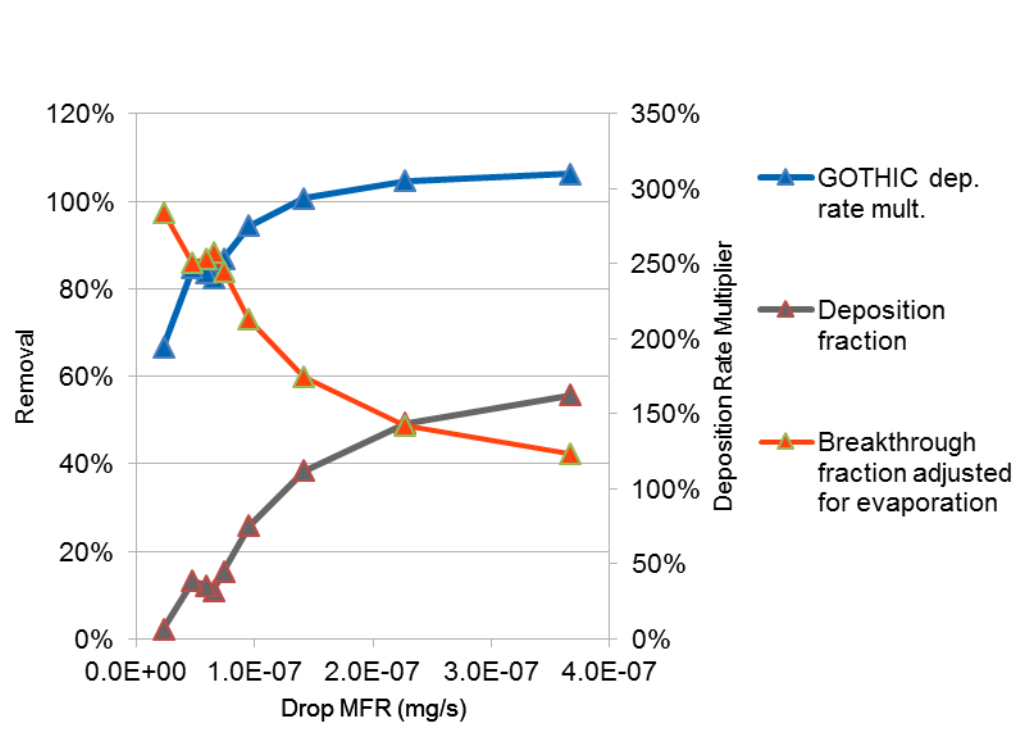
Figure 5.9 Drop Deposition and Breakthrough Fractions and Deposition Rate Parameter

This page is intentionally left blank.

6.   DRY CASK MODEL

DCSS for SNF are designed to provide a confinement barrier that prevents the release of radioactive material, maintain SNF in an inert environment, provide radiation shielding, and maintain subcriticality conditions. SNF is initially stored in pools of water for cooling where the water also provides radiation shielding. As these pools get closer to capacity, dry storage systems are becoming the primary alternative for interim storage. After sufficient cooling in pools, SNF is loaded into a canister and the canister is welded shut. Then the DCSS is decontaminated and dried. The canister is placed into a storage module and then moved to an independent spent fuel storage installation. Figure 6.1 shows the major components of a DCSS for SNF. Typically, the canisters are made of stainless steel. The open volume between the canisters and the cask allows passive ventilation from outside air, which can include dust that collects on the surfaces of the canister. As the SNF cools, salts contained in the dust may deliquesce to form a concentrated brine, which may contain corrosive species such as chlorides. These species are capable of causing localized corrosion, called pitting. With sufficient stresses, these pits can evolve into SCCs, which could penetrate through the canister wall and allow communication from the interior of the canister to the external environment (Schaller et al. 2017).

6.1   Description of the Dry Cask Storage System

A modern DCSS consists of a concrete cask (CC) and a welded stainless-steel dry storage canister (DSC) with a welded closure to safely store spent nuclear fuel. The CC hosts the DSC in its central cavity and provides structural protection, radiation shielding, criticality control, and the necessary cooling to remove the decay heat from the stored fuel in the DSC by natural circulation. A schematic of a typical, commercial DCSS is depicted in Figure 6.1.
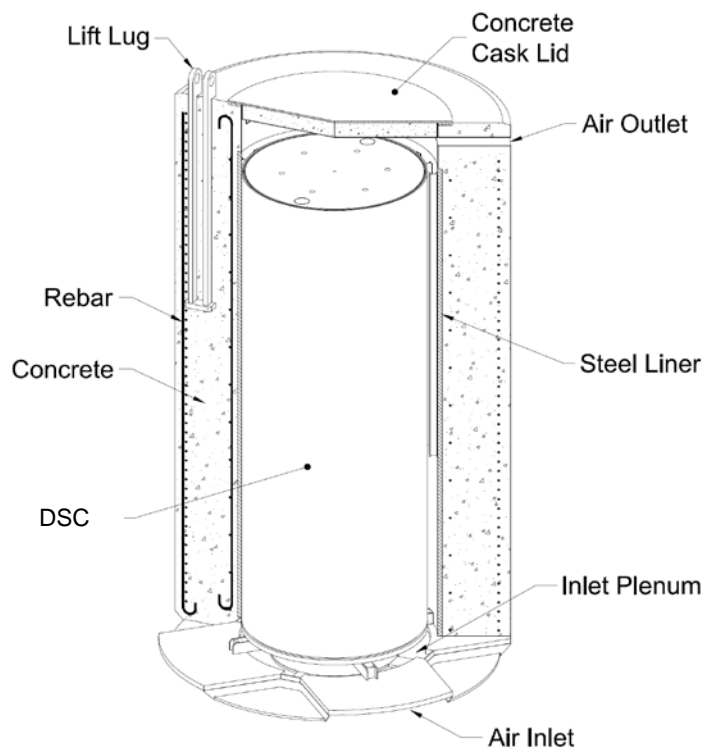

Figure 6.1. Dry Cask Storage System

The DSC contains a pressurized water reactor (PWR) fuel basket which positions and supports up to 37 PWR fuel spent assemblies. The structural components of the basket are fabricated from ASME SA537 Class I carbon steel and coated with nickel plating to minimize corrosion. To maintain subcriticality of the configuration, neutron absorber panels and stainless steel retainers are installed on the basket structure.

Fuel assemblies are stored within the fuel basket in square fuel tubes which are held in a right-circular cylindrical configuration using support weldments that are bolted to the outer fuel tubes. The DSC is backfilled with pressurized inert helium (7 atmospheres) to provide corrosion protection for fuel cladding and enhance heat transfer for the stored fuel.

The concrete cask, designed to hold the DSC, is a reinforced structural plain concrete shield wall with a structural, S beam-shaped steel inner liner that provides neutron and gamma shielding for the stored spent fuel. The inner liner of the CC incorporates standoffs that help to center the canister in the CC. The air in the annular space between the DSC and the CC is naturally circulated around the DSC to remove the decay heat from the stored fuel assemblies. The steel-lined penetrations at the top and bottom of the concrete body of the cask provide paths for air to flow in and out of the CC. The air flow inside the CC is directed in the upward direction and around the pedestal plate by the weldment baffle.

The heat transfer inside the DSC (from fuel assemblies to structural materials) is through conduction, convection, and radiation. The increased helium density due to pressurization enhances convective heat transfer inside the DSC while the CC is passively cooled by naturally circulating air in the annular space between the DSC and the CC. Ambient air enters at the bottom of the CC through four air inlets and heated air exits through the top air outlets due to natural convection heat transfer. Radiant heat transfer occurs from the DSC surface to the CC steel liners, which subsequently transfers heat to the circulating air in the CC annular space. This natural circulation of air along with the associated heat transfer cool down the fuel assemblies inside the DSC and keep the clad and CC component temperatures below their design limits.

6.2   Radial and Axial Assembly Decay Heats

Decay heat from the stored fuel assemblies provides the principal heat load in the thermal analysis of the DCSS. This decay heat, which is a direct result of fuel irradiation (burnup) inside the reactor for extended periods of time, must be continuously removed from the inside of the storage system to maintain the clad and cask component temperatures below their design limits.

For the current analysis, Fort et al. (2016) and the references therein provide a detailed description of a computational approach used for estimating assembly decay heats. The computational approach is based on the processing of pin-by-pin data, obtained from Duke Energy (plant operator), using the ORNL ORIGAMI tool. The results of these calculations are referred to as "best estimate" values and will provide the heat load for the thermal analysis of the DCSS presented in this report.

Figure 6.2 shows the best estimate radial distribution of assembly decay heats at the initial loading used in the current analysis.

	626.66	620.82	423.84		

Figure represents radial distribution grid:

		626.66	620.82	423.84		
	630.54	854.37	796.00	854.67	413.78	
661.31	850.57	784.67	751.95	703.88	818.99	664.12
663.32	846.64	754.10	757.81	697.24	819.21	683.34
675.28	833.97	769.34	697.44	882.76	854.37	672.24
	416.89	867.83	802.50	892.98	647.53	
		415.35	661.95	646.74		

Figure 6.2 Radial Distribution of Assembly Decay Heats (in Watts) for Initial Loading (Best Estimate)

Because fuel burnup inside the reactor is not radially or axially uniform, the decay heat of fuel assembly is expected to follow same trend as fuel burnup. Physically, these nonuniformities in fuel burnup are a direct consequence of radial and axial leakage of neutrons from the finite reactor core (end effect). The discrepancy between the axially dependent burnup analysis and the uniform analysis is a function of the axial burnup profile (power history of the assembly), axial reflector, cask configuration, fuel assembly length, and cooling time.

To calculate a limiting axial burnup profile for PWR fuel assemblies that can be used in thermal analyses of DCSS, a calculation procedure is outlined in (DOE 1977), which describes the processing of 3169 axial burnup profiles from five different PWR fuel types that represent 20 different PWR reactors and 105 operating cycles.

The resulting limiting burnup profiles are tabulated as 18 normalized equal-size nodes and are functions of the assembly average burnup. Table 6-1 was adopted from DOE (1977). In the current thermal analysis, axial burnup profile 3 was used as representative for high burnup fuels.

Table 6-1 Limiting Axial Burnup Profiles

Axial Position (% of active core height)	Normalized Burnup		
	Profile 1 BU < 18 GWD/MTU	Profile 2 18 < BU < 30 GWD/MTU	Profile 3 BU > 30 GWD/MTU
2.78	0.646	0.668	0.652
8.33	1.044	1.034	0.967
13.89	1.208	1.150	1.074
14.99	1.215	1.094	1.103
25.00	1.214	1.053	1.108
30.56	1.208	1.048	1.106
36.11	1.197	1.064	1.102
41.67	1.189	1.095	1.097
47.22	1.188	1.121	1.094
52.78	1.192	1.135	1.094
58.33	1.195	1.140	1.095
63.89	1.190	1.138	1.096
69.44	1.156	1.130	1.095
75.00	1.022	1.106	1.086
80.56	0.756	1.049	1.059
86.11	0.614	0.933	0.971
91.67	0.481	0.669	0.738
97.22	0.284	0.373	0.462

BU = burnup; GWD/MTU = gigawatt-days per metric ton of uranium

6.3 **Fluid Flow Modeling**

The GOTHIC model of the DCSS is composed of a collection of volumes that correspond to actual spaces inside the cask, connected by flow paths and/or thermal conductors to facilitate momentum, mass, and thermal energy transfer between adjacent volumes depending on their local conditions. Figure 6.3 shows a schematic of the volume representations of DSC and CC compartments in GOTHIC. The upper and lower plena of the DSC and CC are constructed with lumped volumes (marked as 38, 39, 40, 42, and 43 on Figure 6.3). Alternatively, subdivided volumes were used to model fuel tube volumes and the CC annulus region to allow for greater details inside these volumes. Of special interest was the ability to model the fuel assembly within a fuel tube with the porous media approach. Subdivided volumes enable calculations for the circulating helium inside the DSC, modeling the axial decay heat as prescribed by Profile 3 (Table 6-1), and verification of the natural circulation cooling mechanism in the CC annulus.

Figure 6.4 shows a front view of a subdivided volume representing a fuel tube where shaded areas indicate locations of cells with specified porosities. Although this figure is not to scale, it depicts the fuel tube height and discretization, as the volume is displayed in the GOTHIC user interface. Cell porosities were calculated based on the total volume of the cell and the volume of all flow blockages inside that cell. Flow blockages refers to fuel assembly structures that displace free volume within the tube.
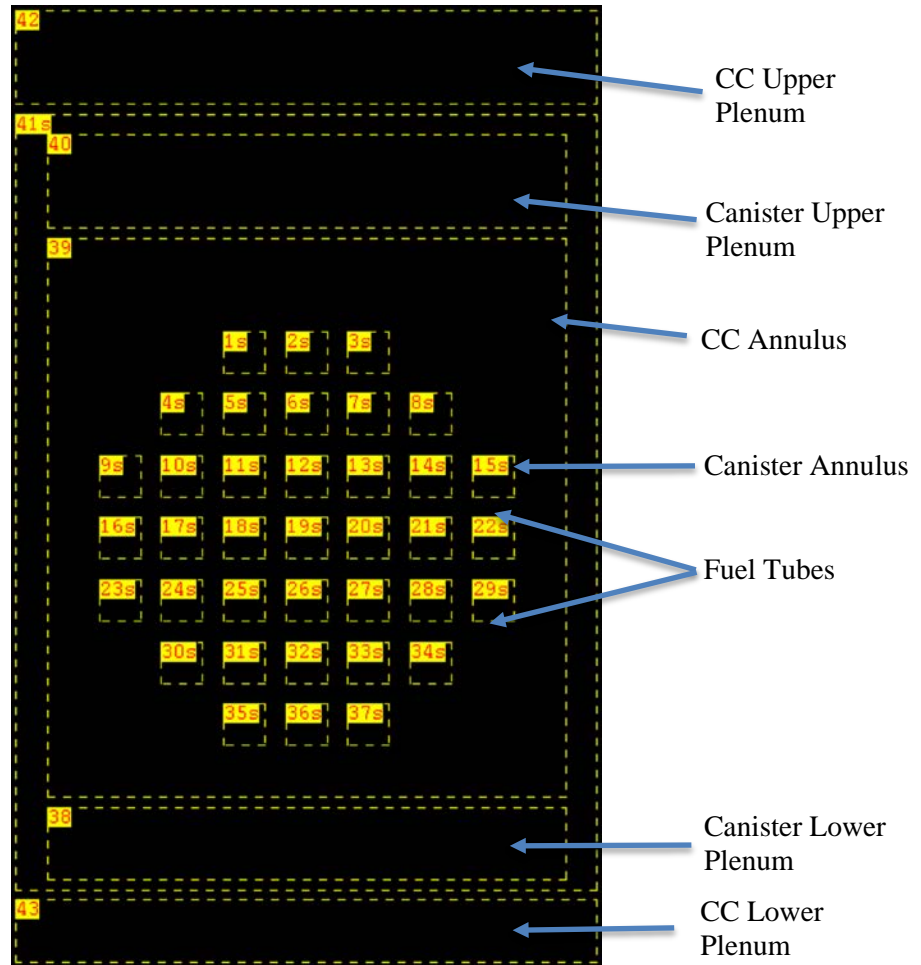
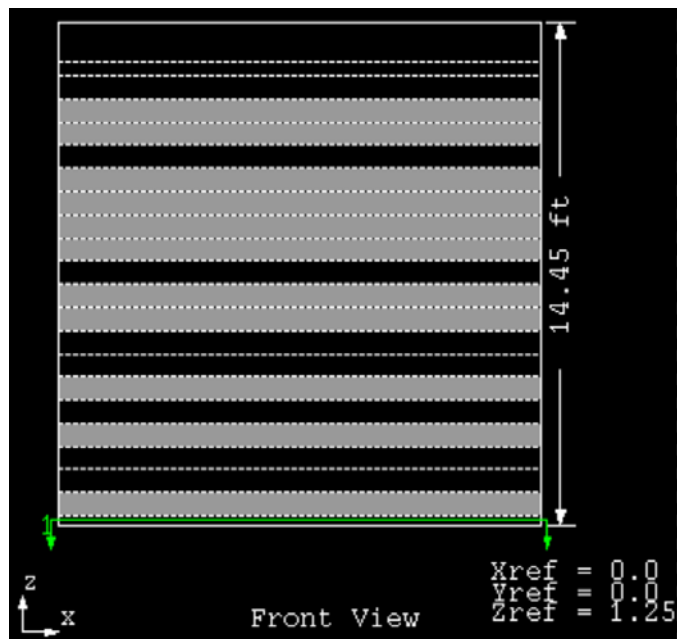**Figure 6.3 Canister and CC Volume Representations in GOTHIC**

Figure 6.4 Representation of a Fuel Tube Using GOTHIC's Subdivided Volume

The upper and lower plena of the DSC were connected to the DSC annulus using the flow path modeling element of GOTHIC to allow for natural circulation of helium between the basket and the canister shell. The fuel tubes were also connected to the DSC upper and lower plena to allow for the cooling of the fuel assemblies.

Cooling air was allowed to enter and exit the CC lower and upper plena by applying the appropriate boundary conditions as discussed later.

6.4 **Heat Transfer Modeling Elements**

To allow for heat transfer between adjacent volumes in the cask model, GOTHIC provides thermal conductor modeling elements which can be defined where heat transfer is likely to occur. Thermal conductors can also be used to model volumetric heat generation inside the volumes containing the conductors. When a conductor is defined in GOTHIC, pre-defined surface options and conductor types are used to specify the modes of heat transfer on the surfaces of the conductor and its geometry. Figure 6.5 shows a schematic of the thermal conductors defined in the cask model.
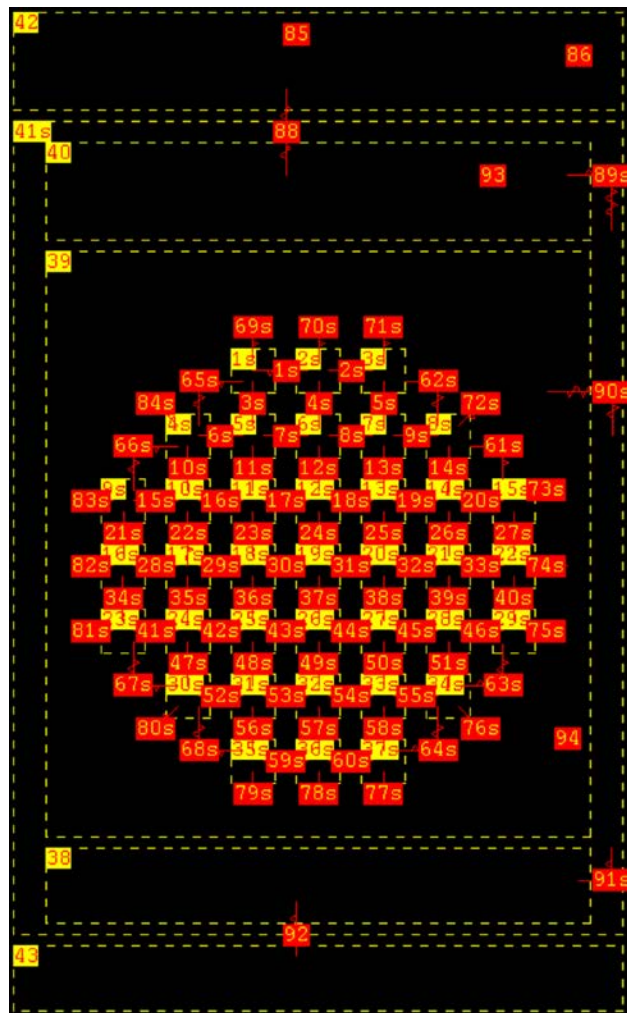

Figure 6.5 Thermal Conductors in the Cask Model

Several types of thermal conductors were defined in the cask model to account for conductor's geometry and material. Depending on the heat transfer conditions on both sides of the conductor, a 1-D discretization can also be added to the conductor type definition that will be used by GOTHIC to solve the

heat transfer equation. Thermal conductors of various types (i.e., geometries) were used to model heat transfer between difference components of the model. For example, wall conductor type was used to model heat transfer between adjacent fuel tubes inside and on the periphery of the basket, whereas tube conductor type was used to model heat transfer in the CC annular space.

Of special interest are the rod conductor types, which represent the decay heat generation in the central assembly (subdivided control volume # 19 in Figure 6.3).

6.5   Axial Decay Heat Modeling

As mentioned earlier, the best-estimate assembly decay heat at the initial loading and burnup Profile 3 (Section 6.2) were used to specify the heat load for the current thermal analysis of the cask. Apart from the central assembly (subdivided volume # 19 in Figure 6.3), GOTHIC's heater modeling element was used to model decay heat generation in fuel assemblies. The total heat load using this best-estimate decay heat loading is 26.415 kW.

Figure 6.6 shows the axial decay heat profiles used for assemblies # 16, 17, and 18. The axial profiles shown in Figure 6.6 are consistent with the design basis decay heat loading define in Fig. A-1 of Fort et al. (2016).
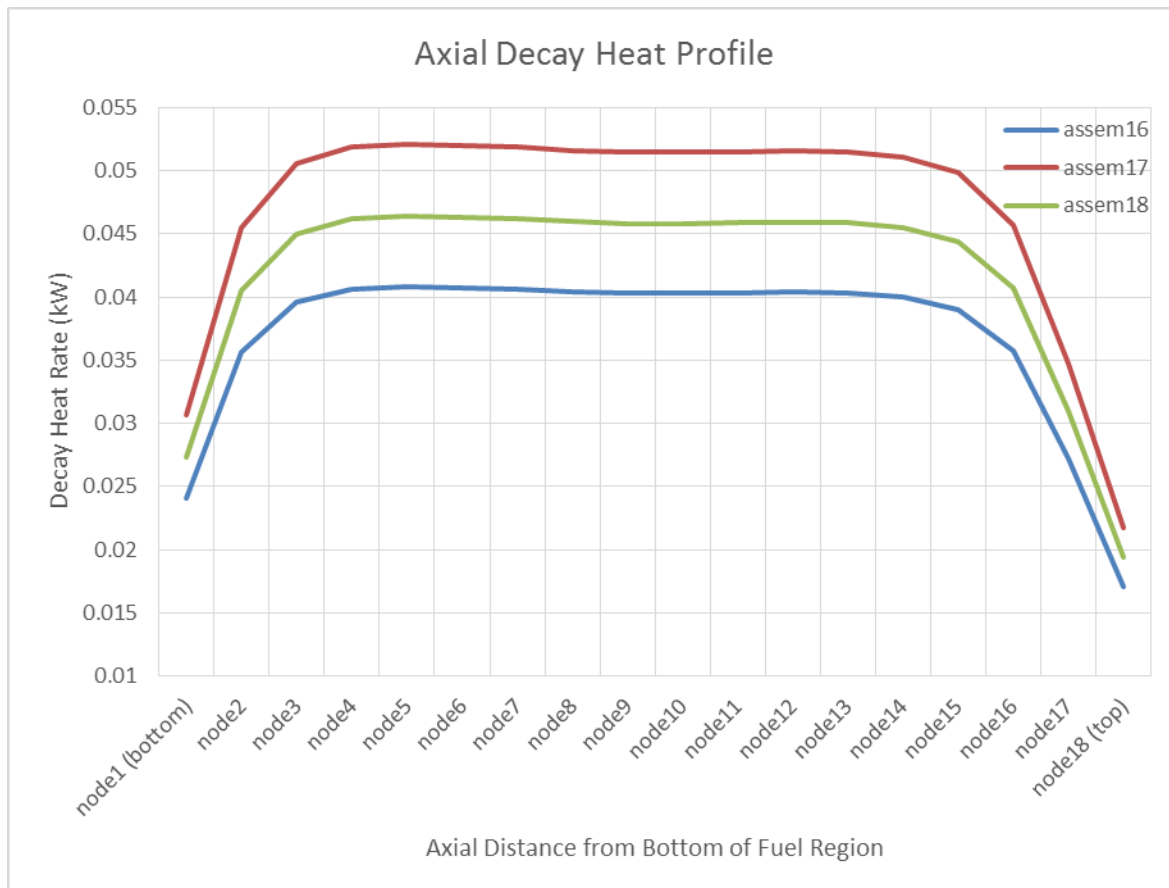

Figure 6.6   Axial Decay Heat Profile for Assemblies # 16, 17, and 18

6.6   Initial/Boundary Conditions

The cask model was initialized with air at 101.3 kPa (14.7 psia) and 76 $^\circ$F (25 $^\circ$C) in all CC volumes (CC upper and lower plena and CC annulus) and with pressurized helium at 709.3 kPa (102.9 psia) in the DSC volumes (DSC upper and lower plena, DSC annulus, and fuel tubes).

Other initial conditions were implicitly entered during the definition of other modeling entities. These were mostly related to defining the initial temperatures of thermal conductors.

To initialize the flow of cooling air at the inlets of the cask, a flow boundary condition was defined, which specifies a mass flow rate of 0.68 kg/sec at 25 $^\circ$C (76 $^\circ$F) and 101.3 kPa. A pressure boundary condition was also applied at the CC air outlets. The completed GOTHIC model of the cask is shown in Figure 6.7.
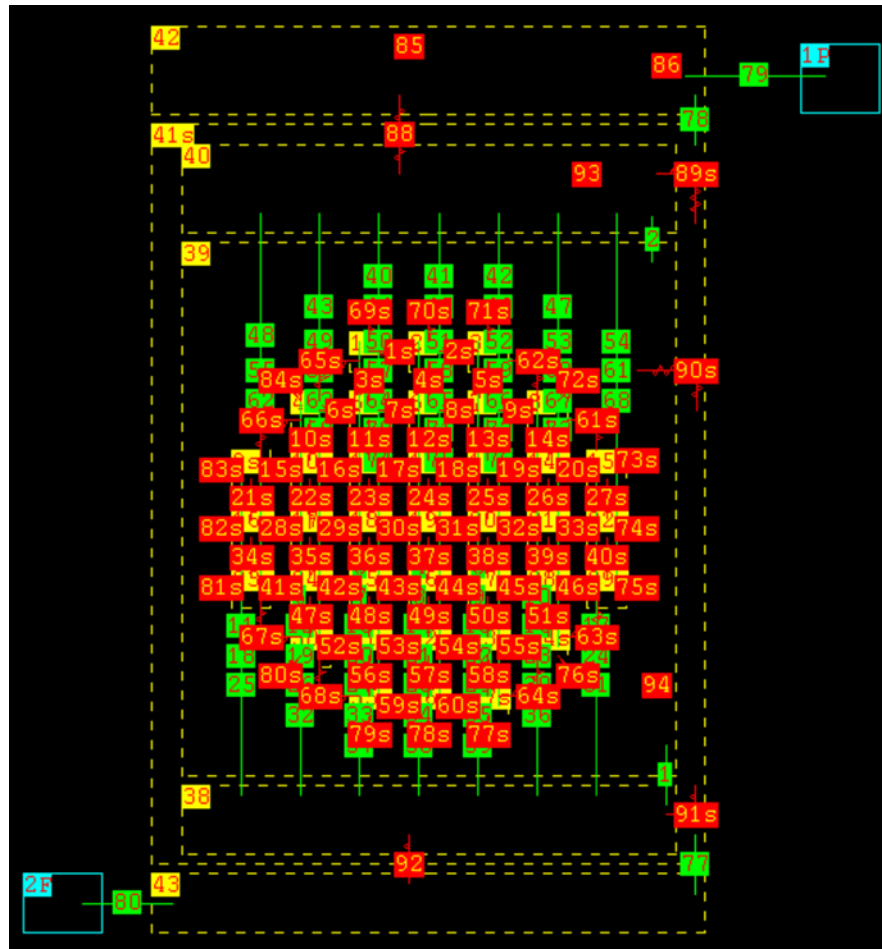

Figure 6.7   Completed GOTHIC Model of the MAGNASTOR Cask

6.7   Results and Discussion

This section summarizes the results of the thermal analysis of the DCSS using GOTHIC. As mentioned earlier, the thermal loads used in this analysis are those described axially by Profile 3 in Table 6-1 and radially by the best-estimate assembly decay heats as illustrated in Figure 6.2.

The results discussed here are steady state solutions for flow and temperature. Although GOTHIC is not a steady state solution code, the authors approached steady state conditions by judiciously choosing initial

conditions and then running the simulation until flows and temperature stabilize in response to the boundary conditions.

To compare the GOTHIC model prediction of PCT in the hot channel of the DCSS against COBRA-SFS and STAR-CCM+ predictions, the central assembly decay heat generation was modeled by a conductor that generates heat with an axial distribution in place of heaters, which were used to model decay heat generation in other assemblies in the cask. Axial dependent decay heat distributed over the vertically subdivided hot channel volume allows for the calculation of the PCT of the average fuel rod in the central assembly. The result of the PCT calculation at the central assembly (in GOTHIC subdivided volume # 19 in Figure 5.3) is summarized in Table 6-2.

Table 6-2 Comparison of GOTHIC Against COBRA-SFS and STAR-CCM+ Results for PCT Calculation

Code	PCT, °C (°F)	% rel. err.[a]
GOTHIC	306.7 (584.1)	-
COBRA-SFS	301 (573.8)	1.9
STAR-CCM+	307 (584.6)	-0.1

[a]% rel. error $= (GOTHIC - Code) \times 100/Code$

The GOTHIC's PCT result for the central assembly is in excellent agreement with STAR-CCM+ and to a lesser degree with COBRA-SFS result. The fuel thermal structure model includes a radial discretization of the fuel pellet and cladding. The PCT, which occurs at the interface of the central region of the fuel rod (UO$_2$) and the clad (Zircaloy-4), is well below the regulatory limit of 400 °C (752 °F).

Figure 6.8 shows the GOTHIC-predicted radial distribution of helium temperature at the top of the fuel region (hot spot in a fuel tube). The maximum temperature is 310 °C.
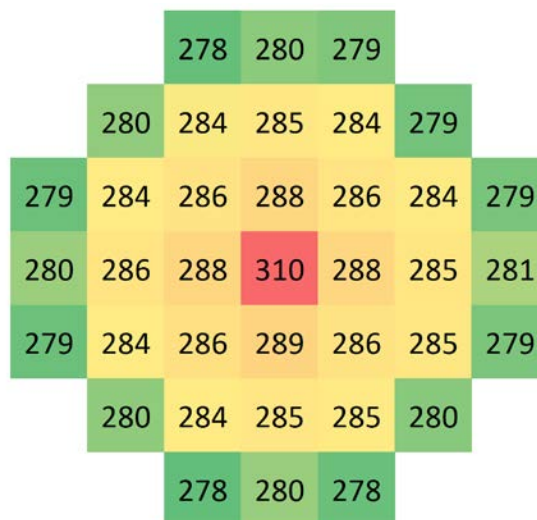

Figure 6.8 Steady State Helium Temperature Distribution at the Top of Fuel Tubes (°C)

Figure 6.9 shows contour plots of the helium gas temperatures inside the DSC in the radial and axial directions.
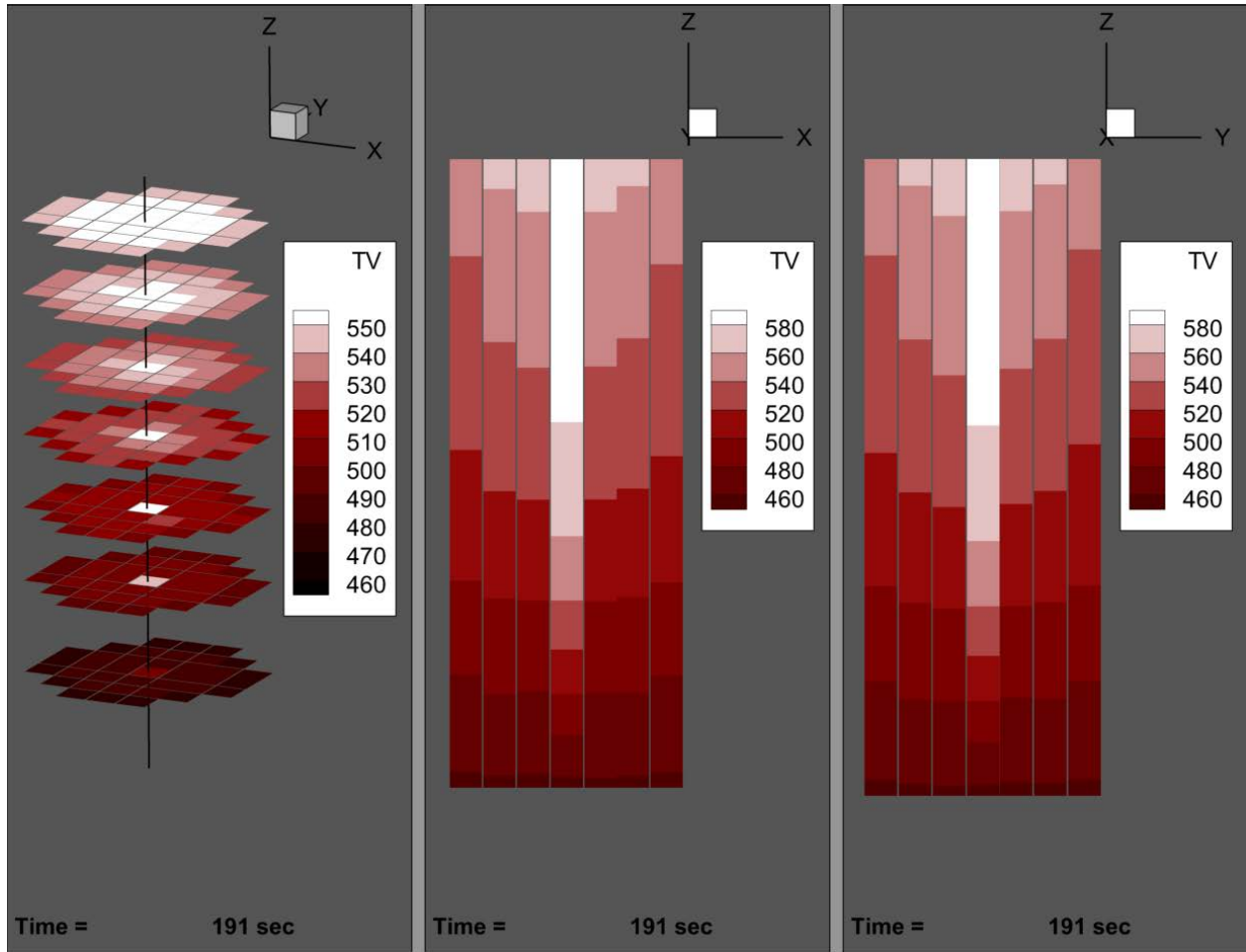

Figure 6.9 Steady State He Temperature (°F) in Canister Tubes

Figure 6.10 shows the velocity vectors of air in the CC annular region. The maximum magnitude of air velocity in the CC annulus is about 1.02 m/sec (3.35 ft/sec), which is in excellent agreement with STAR-CCM+ result (about 1 m/sec). The direction of air velocity vectors indicates the natural circulation of cooling air flowing through the CC annular space.
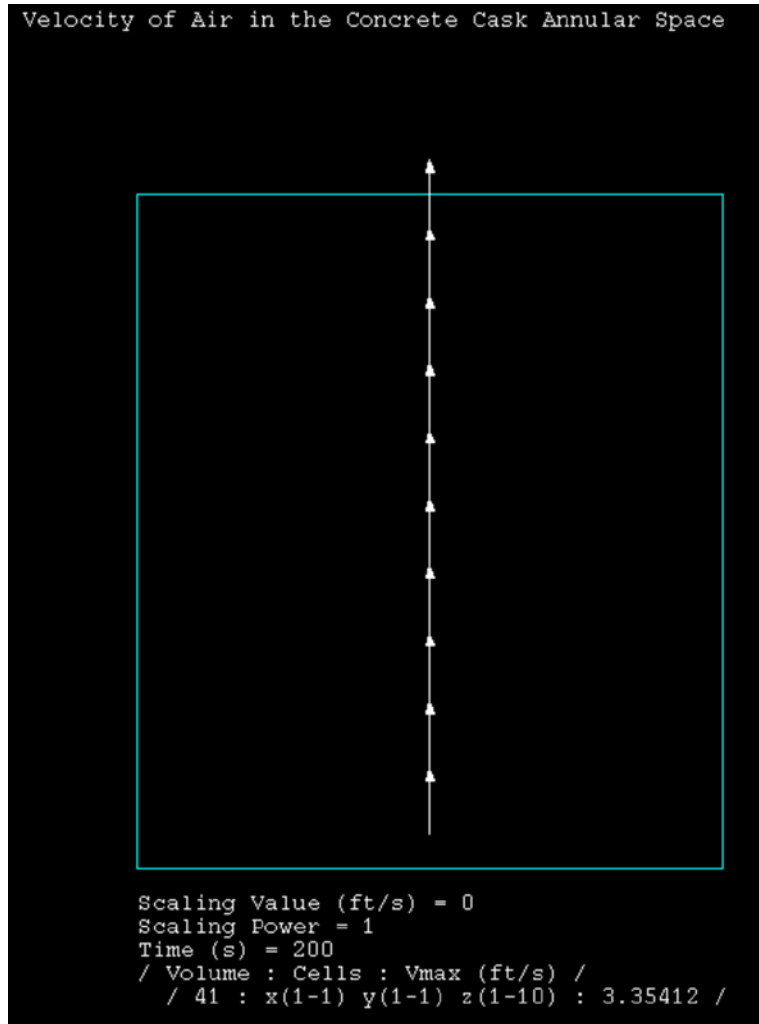

Figure 6.10 Magnitude and Direction of Air Velocity Vectors in the CC Annulus

This page is intentionally left blank.

7.   CONCLUSIONS

The objective of the work leading up to this report was to use GOTHIC to 1) establish a dry cask model that could be compared against existing models and 2) establish a flow model through a microbreach that could be used to characterize aerosol flow through the experimental setup established at SNL. To this end, the initial objective has been met. However, additional work is needed to refine the modeling methods and to combine the two independent modeling tasks into a fully integrated model.

Currently, agreement between the experiment deposition results presented in Durbin et al. (2018) and those predicted by GOTHIC was achieved by increasing GOTHIC deposition rates by a factor of 1.95 to 3.10. The primary difficulty in predicting deposition was the use of a wet aerosol model to simulate a dry aerosol due to a code limitation that prohibited use of the solid component dry aerosol model in the code version initially selected for this work[c].

A detailed model of a SNF storage system was developed and validated by comparison to similar calculations from independent analytic models. Excellent agreements between GOTHIC and other well-established codes were observed. The cask model will be further developed to allow for comparison of additional parameters.

Moving forward, the refinement and integration of the modeling efforts described in this report will proceed in a close collaboration with the modeling efforts at ORNL and the experimental efforts at SNL. The insights provided by the phenomenological modeling at ORNL will help to identify proper flow regime and friction factor assessments in the GOTHIC package and the experimental results from SNL will provide the real-world basis against which the model will be benchmarked and optimized.

---

[c] This problematic limitation has been corrected in the newer version of GOTHIC (8.3), however our work began prior to the release of version 8.3.

This page is intentionally left blank.

8. FUTURE WORK

A simplified approach was taken for fuel representation and tube spatial discretization for tubes in the cask model except the hot fuel tube (tube channel with maximum fuel decay heat). The simplified approach allowed a more rapid development time while conserving the total decay heat and cask volume. In the future, the cask model will be updated with more detailed volumes for the fuel tubes—axial discretization in all tubes will be established to match the hot fuel tube and the fuel in all tubes will be represented by distributed thermal structures representing the resident fuel. A detailed cask model with radial and axial decay heat loading and increased spatial detail will be useful for detailed calculations of temperature and flow conditions within the cask. In addition, future calculations will include cask internal pressure and validation of this parameter from the available literature.

The microchannel and cask models will be updated to GOTHIC Version 8.3, which includes dry aerosol modeling capability, and additional work to evaluate the deposition models in GOTHIC will be performed. The authors hope to collaborate with the experimentalists to obtain more information about the microchannel experiment to enable further refinements of the model. Further development plans for the microchannel model include validation of GOTHIC to predict deposition by impaction in breaches that are not straight.

Future work should investigate aerosol behavior inside a SNF DSC. The analysis should examine the behavior of different particle sizes in a natural convection flow environment. Specifically, the authors are interested to investigate the spatial and size distribution dependence of aerosol settling and deposition as well as the importance of reentrainment of settled and deposited particles from a postulated source term.

Coupling of the cask with a microchannel (or postulated SCC) model in the future will provide a realistic simulation of cask depressurization and internal mixing coupled with the microchannel release flow. The models may be combined into a single model or coupled by data transfer between the models running simultaneously. A known challenge associated with the former approach arises from the large difference in length scales present in the models. The Courant limited time step size of the microchannel model, due to very small spatial discretization, will present a global time step size limit on the combined model, resulting in longer computer time. Another option involves running the models separately and iteratively to converge the solution of cask pressure and the breach mass and energy release.

This page is intentionally left blank.

9.   REFERENCES

Chapman AJ and WF Walker. 1971. *Introductory Gas Dynamics*. Holt, Rinehart and Winston, Inc., New York.

Casella AM, SK Loyalka, and BD Hanson. 2014. "Modeling of Particulate Behavior in Pinhole Breaches." *Nuclear Technology*, 186:99-114. http://dx.doi.org/10.13182/NT13-55.

Chatzidakis, S. 2018. *SCC Aerosol Transport Model Summary Report. M3SF-18OR01201082* ORNL/SPR-2018/1072. Oak Ridge National Laboratory, Oak Ridge, Tennessee.

DOE – U. S. Department of Energy. 1997. Topical Report on Actinide-Only Burnup Credit for PWR Spent Nuclear Fuel Packages. DOE/RW-0472, Office of Civilian Radioactive Waste Management, U.S. Department of Energy. Washington D.C.

Durbin S, E Lindgren, and R Pulido. 2018. *Measurement of Particulate Retention in Microchannel Flows*. SAND2018-10522 R, Sandia National Laboratories, Albuquerque, New Mexico.

Fort J, TE Michener, SR Suffield, and DJ Richmond. 2016. *Thermal Modeling of a Loaded Magnastor Storage System at Catawba Nuclear Station*. FCRD-UFD-2016-000068, PNNL-25871 R0. Fuel Cycle Research and Development, Used Fuel Disposition Campaign, U.S. Department of Energy, Washington, D.C.

Hinds W. 1982. *Aerosol Technology, Properties, Behavior and Measurement of Airborne Particles*. John Wiley and Sons, New York.

Incropera, FP, DP Dewitt, TL Bergman, and AS Lavine. 2007. *Fundamentals of Heat and Mass Transfer*. 6th edition, John Wiley and Sons, New Jersey.

Jenkins SG. 1988. "The Mean Free Path." *Journal of Aerosol Sciences*, 19(2):159-166.

Hirschfelder JO, Curtis CF, Bird RB (1954). *Molecular Theory of Gases and Liquids*. John Wiley and Sons, New York.

GOTHIC Thermal Hydraulic Analysis Package, *Version 8.2(QA)*. EPRI, Palo Alto, CA: 2016.

Michener TE, DJ Richmond, DR Rector, JM Cuta, and HE Adkins. 2019. *COBRA-SFS: A Thermal-Hydraulic Analysis Code for Spent Fuel Storage and Transportation Casks Version 5.0*. PNNL-28421, Pacific Northwest National Laboratory, Richland, Washington.

NAC International. 2015. *MAGNASTOR Final Safety Analysis Report*. FSAR, Rev. 7, Norcross, Georgia.

Schaller RF, A Mishra, JM Rodelas, JM Taylor, and EJ Schindelholz, A. M. 2018. "The Role of Microstructure and Surface Finish on the Corrosion of Selective Laser Melted 304L." *Journal of the Electrochemical Society*, 165(5):C234-C242. https://doi.org/10.1149/2.0431805JES